Optics Letters

Ratiometric 4Pi single-molecule localization with optimal resolution and color assignment

Jianwei Chen,[1,2,†] Benxi Yao,[1,†] Zhichao Yang,[1,3] Wei Shi,[1] Tingdan Luo,[1] Peng Xi,[1,4] Dayong Jin,[1,3] and Yiming Li[1,*]

[1]Department of Biomedical Engineering, Southern University of Science and Technology, Shenzhen 518055, China
[2]Harbin Institute of Technology, Harbin, 150001, China
[3]Institute for Biomedical Materials and Devices (IBMD), Faculty of Science, University of Technology Sydney, NSW 2007, Australia
[4]Department of Biomedical Engineering, College of Future Technology, Peking University, Beijing 100871, China
*Corresponding author: liym2019@sustech.edu.cn
†These authors contributed equally to this work.

Received 27 October 2021; revised 9 December 2021; accepted 12 December 2021; posted 13 December 2021; published 7 January 2022

4Pi single-molecule localization microscopy (4Pi-SMLM) with two opposing objectives achieves sub-10 nm isotropic 3D resolution when as few as 250 photons are collected by each objective. Here, we develop a new ratiometric multi-color imaging strategy for 4Pi-SMLM that employs the intrinsic multi-phase interference intensity without increasing the complexity of the system and achieves both optimal 3D resolution and color separation. By partially linking the photon parameters between channels with an interference difference of π during global fitting of the multi-channel 4Pi single-molecule data, we show via simulated data that the loss of localization precision is minimal compared with the theoretical minimum uncertainty, the Cramer–Rao lower bound.

https://doi.org/10.1364/OL.446987

In the past decade, single-molecule localization microscopy (SMLM) [1,2] has revolutionized the field of biological imaging by improving the resolution of conventional fluorescence microscopy by more than an order of magnitude, achieving nanometer-scale imaging resolution. In particular, imaging schemes incorporating two objective lenses to coherently detect single-molecule fluorescence in a 4Pi geometry have been shown to improve the axial resolution dramatically, even surpassing the lateral resolution [3]. The high axial sensitivity is due to the fact that the interference phase of the single molecule directly couples with the axial position, resulting in a fast change in the intensity of the 4Pi point spread function (PSF) along the axial direction. By comparing the intensities of single molecules in the three [4] or four [5–7] interference phase channels, one can get a very sensitive readout of a single molecule's axial position. Therefore, by combining SMLM with 4Pi detection, near-isotropic resolution down to approximately 10 nm has been achieved [4–6,8].

Multi-color SMLM is crucial to investigations of the spatial relationship among different biomolecules. Different multi-color strategies have been applied in combination with SMLM [9,10]. Ratiometric multi-color imaging can distinguish the colors of spectrally similar single molecules using the relative intensity information from two spectral channels split by a dichroic mirror [11]. This approach has several advantages over conventional multi-color imaging using spectrally distinct dyes: (1) many of the best 'blinking' dyes for SMLM are far-red dyes; (2) chromatic aberration can be neglected, which is important for ultrahigh-resolution multi-color imaging; and (3) only one laser is utilized to perform simultaneous multi-color imaging. However, a conventional photometry-based method is not suitable to perform ratiometric color assignment, as the intensity information is used to determine the interference phase. The first approaches to using ratiometric multi-color imaging in 4Pi-SMLM employed the intensity difference between the p- and s-polarization channels by placing a dichroic mirror in front of the camera at a special angle [5,12]. Recently, Zhang *et al.* solved this problem by using an additional camera to collect the salvaged fluorescence reflected by the main excitation dichroic mirror, and determined the color from the intensity ratio between the salvaged fluorescence and normal fluorescence [13]. However, this approach comes at the cost of increased hardware complexity.

The latest developments in 4Pi-SMLM have involved the introduction of spline-interpolated PSF models [14] to directly fit the 4Pi single-molecule data instead of photometry-based methods, allowing an analytic model to accurately describe the fringe-like 4Pi-PSF [15,16], and achieving the Cramer–Rao lower bound (CRLB) in both simulated and experimental 4Pi single-molecule data. Since 4Pi single-molecule imaging is intrinsically collected in multi-interference channels, we hypothesized that one could perform regular ratiometric multi-color imaging among different interference channels, thus achieving multi-color 4Pi-SMLM without adding additional detection channels.

Figure 1(a) is the optical design proposed for our ratiometric multi-color 4Pi-SMLM. We followed the work of Huang *et al.* [6] and introduced four interference channels by separating the p- and s-polarization channels with a phase shift of $\pi/2$. In order to perform ratiometric multi-color imaging between these channels, we then inserted filters into one or two of the interference channels after the beam splitter (BS) to create an intensity difference between channels for spectrally different dyes, as shown

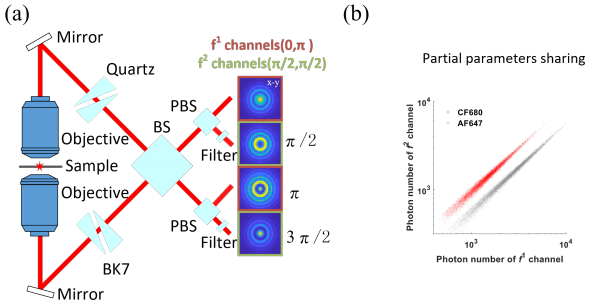

Fig. 1. Schematic of the ratiometric multi-color 4Pi-SMLM employing intrinsic multi-phase interference channel detection. (a) Schematic of the 4Pi-SMLM microscope. The emitted fluorescence is collected by upper and lower objectives. Before self-interference occurs at the 50/50 beam splitter (BS), the phases of p- and s-polarized fluorescence are shifted by two modified Babinet–Soleil compensators so that four-phase interference channels (0, $\pi/2$, π, and $3\pi/2$) are detected simultaneously. The four-phase channels are then separated by a polarizing beam splitter (PBS) and collected at different regions of one camera. One or more filters are inserted into the f^1 (0, π) or f^2 ($\pi/2$, $3\pi/2$) interference channels to create an intensity difference for spectrally different dyes. (b) Scatter plot of the photons in the f^1 and f^2 channels for the AF647 (bottom line) and CF680 (top line) dyes separately.

in Fig. 1(b). We finally used the intensity difference for each molecule to determine its color information.

To achieve the theoretical limit of 3D localization precision (the CRLB) for 4Pi-SMLM, we adopted the experimental IAB-based 4Pi-PSF model [15]. The experimental 4Pi-PSF model is defined as $P(x, y, z, \varphi) = I + A\cos(\varphi) + B\sin(\varphi)$. Here, $I(x, y, z)$, $A(x, y, z)$, and $B(x, y, z)$ are slowly varying functions of x, y, z and are independent of the interference phase φ. We then divide the interference channels into two classes:

$$f_{ki}^1(x, y) = \theta_{NP1} P(x - \theta_x, y - \theta_y, \theta_z, \theta_\varphi + \phi_i) + \theta_{bgi}, \quad (1)$$

$$f_{kj}^2(x, y) = \theta_{NP2} P(x - \theta_x, y - \theta_y, \theta_z, \theta_\varphi + \phi_j) + \theta_{bgj}. \quad (2)$$

Here, f_{ki}^1 and f_{kj}^2 are the expected intensity value of the kth pixel at position (x, y) in the ith and jth channel, respectively. The f^1 channels all have the same photon number θ_{NP1}, while the f^2 channels all have the same photon number θ_{NP2}. In this work, we insert a filter into the f^2 channels to create an intensity difference between the f^1 and f^2 channels so that ratiometric multi-color imaging can be performed. θ_x, θ_y, θ_z, and θ_φ are the x, y, z positions and the interference phase of the emitter, respectively. They are global parameters and are the same for all channels. θ_{bgi} and θ_{bgj} are the constant background photons per pixel over the extent of the PSF in the ith and jth channel, respectively. ϕ_i and ϕ_j are the corresponding relative phase shift in each channel, which is controlled by the Babinet–Soleil compensators. The estimation of the θ parameters is achieved using maximum likelihood estimation (MLE)-based nonlinear optimization, whose cost function across different channels is defined as

$$\chi_{mle}^2 = \chi_1^2 + \chi_2^2, \quad (3)$$

where

$$\chi_1^2 = 2\sum_i \sum_k (f_{ki}^1 - M_{ki}) - 2\sum_i \sum_k M_{ki} \ln(f_{ki}^1 / M_{ki}), \quad (4)$$

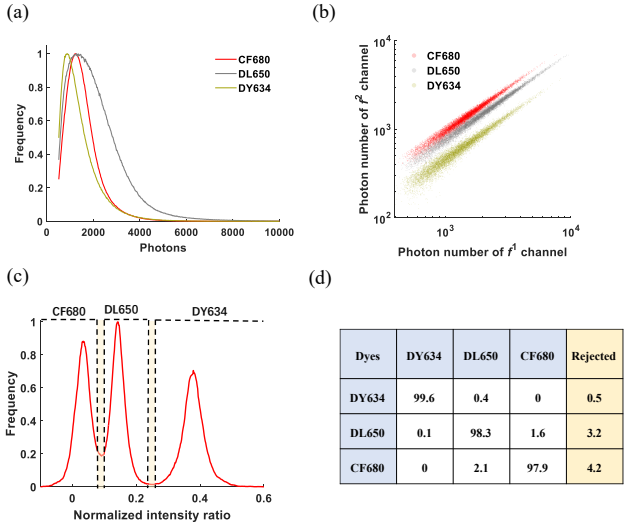

Dyes	DY634	DL650	CF680	Rejected
DY634	99.6	0.4	0	0.5
DL650	0.1	98.3	1.6	3.2
CF680	0	2.1	97.9	4.2

Fig. 2. Color separation of ratiometric 4Pi-SMLM by partially linking the photons in different interference channels during the fitting of multi-channel 4Pi single-molecule data. (a) Experimental photon distributions of CF680 (middle curve), DL650 (right-most curve), and DY634 (left-most curve). (b) Scatter plot of the photons in the f^1 (0 and π) versus f^2 ($\pi/2$ and $3\pi/2$) channels returned by the IAB-based 4Pi-PSF model fit. CF680, top curve; DL650, middle curve; DY634, bottom curve. (c) Normalized intensity ratio between the f^1 and f^2 channels obtained by partially linking photons in the f^1 and f^2 channels separately. The molecules were assigned to three different colors indicated by the three boxed regions. Left to right: CF680, DL650, and DY634. (d) The cross talk (in %) of the three dyes using our proposed ratiometric multi-color 4Pi-SMLM method.

$$\chi_2^2 = 2\sum_j \sum_k (f_{kj}^2 - M_{kj}) - 2\sum_j \sum_k M_{kj} \ln(f_{kj}^2 / M_{kj}). \quad (5)$$

χ_1^2 and χ_2^2 are the negative log likelihood functions for the f^1 and f^2 channels, respectively. M_{ki} is the measured number of photons from the kth pixel in the ith channel. By minimizing χ_{mle}^2, we obtain the maximum likelihood for the Poisson process.

We then evaluated the color separation of our proposed multi-color 4Pi-SMLM approach using simulated data. To allow a comparison, we chose the same dyes as Zhang *et al.* did for three-color super-resolution imaging (CF680, DL650, DY634) [13]. The experimental single-molecule photon distributions of these dyes are shown in Fig. 2(a). To simulate the 4Pi single-molecule data, we employed a full vectorial PSF model [17] and coherently added up the counterpropagating electrical fields from the upper and lower objectives. Here, an ideal 4Pi-PSF was simulated for both the upper and lower objectives with a NA of 1.35. The refractive indices of the immersion medium and the sample medium were both 1.40. The refractive index of the cover glass was set to 1.518. The emission wavelength was set to the central wavelength of DL650 (688 nm). The effect of the wavelength differences between these three dyes on the localization accuracy is negligible (Supplement 1, Fig. 1). An additional astigmatism of $60m\lambda$ was added to both the upper and the lower PSF. The same parameters were used throughout this work unless noted otherwise. We then decomposed the 4Pi-PSF into an IAB-based 4Pi-PSF model that was subsequently used to fit the 4Pi single-molecule data. 10,000 molecules were simulated with x and y positions randomly distributed between

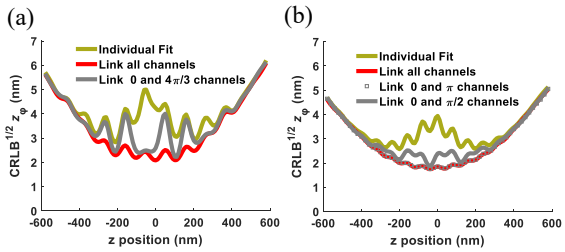

Fig. 3. Comparison of the $\sqrt{\text{CRLB}}\ z_\varphi$ values obtained by partially linking photons between different multi-phase interference channels in (a) three-phase and (b) four-phase interference 4Pi-SMLM. For each phase channel, 1,000 photons/localization and 20 background photons/pixel were used. Top curve, individual fit; bottom curve, link all channels; middle curve, link 0 and $4\pi/3$ channels.

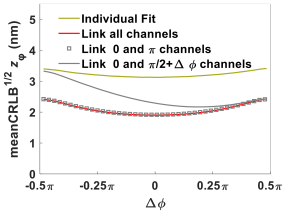

Fig. 4. Theoretical minimum uncertainty of z_φ as a function of the phase shift between the p- and s-polarization channels in four-interference-phase 4Pi-SMLM imaging. Top curve, individual fit; middle curve, link 0 and $4\pi/3$ channels; bottom curve, link all channels.

-1 and 1 pixels from the center of the fitting window and z positions randomly distributed between -600 nm and 600 nm from the focus. Only Poisson noise was added to the images.

We then employed our global fit algorithm [18] to simultaneously fit four channels with x, y, z and phase as global parameters. The fitted photons of the f^1 versus f^2 channels are shown in Fig. 2(b). We then calculated the normalized intensity ratio r between the f^1 and f^2 channels: $r = (\theta_{NP1} - \theta_{NP2})/(\theta_{NP1} + \theta_{NP2})$. The histogram of r is shown in Fig. 2(c). We assigned the molecules to three different colors based on the r threshold indicated by the three boxed regions. Molecules between boxes were rejected (yellow regions). As shown in Fig. 2(d), the cross talk (in %) of the three dyes is less than 4%, while the rejection ratio of the molecules is below 5%. We compared the result with conventional color separation methods using photometry and individual fit methods, and global fitting showed the best performance (Supplement 1, Fig. 2). The cross talk of the color assignment under different light levels was also investigated (Supplement 1, Fig. 3).

In the 4Pi-SMLM imaging, the intensities in different phase channels are normally highly correlated. Therefore, the first approach to localizing the z positions of 4Pi single molecules was to employ the intensity ratio between different channels to determine the interference phase [4–6]. We hypothesized that unlinking the photons between channels could lose information content and thus reduce the localization precision. To investigate the influence of our approach on the localization precision, we calculated the $\sqrt{\text{CRLB}}$ of the x, y, z positions within the z range of 600 nm below to 600 nm above the focus. Here, we compared the localization precision obtained with photons linked/unlinked in all channels to that obtained when they were partially linked between channels. Both three and four interference phase channels were investigated. As expected, when the photon parameter was fitted individually for each channel, $\sqrt{\text{CRLB}}\ z$ was much worse than that obtained when the photon parameter was fitted globally across different channels [Figs. 3(a) and 3(b), yellow and red lines]. $\sqrt{\text{CRLB}}\ x$ and $\sqrt{\text{CRLB}}\ y$ were not affected by the changing the photon-linking scheme used (Supplement 1, Fig. 4).

We then further investigated whether the CRLB could be improved by partially linking the photons within the f^1 and f^2 channels. During the fitting, the photons in the f^1 channels had the same parameter θ_{NP1}, while the photons in the f^2 channels had the same parameter θ_{NP2}. For three-interference-phase-channel 4Pi-SMLM imaging (0, $2\pi/3$, $4\pi/3$), we inserted a filter into one of the channels (i.e., $4\pi/3$). Therefore, the 0 and $2\pi/3$ channels were classed as f^1 channels and the $4\pi/3$ channel was classed as an f^2 channel. We then compared the $\sqrt{\text{CRLB}}\ z_\varphi$ obtained under this partial linking scheme to that obtained under the fully linked condition. Although $\sqrt{\text{CRLB}}\ z_\varphi$ was improved compared to that obtained when the photon was individually fitted, there were some peak positions where $\sqrt{\text{CRLB}}\ z_\varphi$ was much worse than when the photons were fully linked between channels [gray line in Fig. 3(a)]. For four-interference-phase-channel 4Pi-SMLM imaging (0, $\pi/2$, π, $3\pi/2$), we partially linked the photons between channels in two different ways. In the first method, the 0 and $\pi/2$ channels were grouped as f^1 channels, and the π and $3\pi/2$ channels were grouped as f^2 channels. Similar to the three-interference-phase case, there were some peak positions of $\sqrt{\text{CRLB}}\ z_\varphi$ [gray line in Fig. 3(b)]. In the second method, the 0 and π channels were grouped as f^1 channels, and the $\pi/2$ and $3\pi/2$ channels were grouped as f^2 channels. Surprisingly, we found that $\sqrt{\text{CRLB}}\ z_\varphi$ was almost the same as when the photons were fully linked [squares in Fig. 3(b)]. We therefore used this linking scheme for our ratiometric 4Pi-SMLM imaging strategy.

We further systematically evaluated $\sqrt{\text{CRLB}}\ z_\varphi$ for different phase shifts $\Delta\phi$ relative to $\pi/2$ between the p and s channels to find an optimal $\Delta\phi$ that could achieve the theoretical best localization precision (Fig. 4). We obtained the mean $\sqrt{\text{CRLB}}\ z_\varphi$ for z positions in the range $\pm$ 200 nm around the focus using four different parameter sharing schemes: link/unlink photons in all channels, partially link the photons in the 0 and π channels, or partially link the photons in the 0 and $\pi/2+\Delta\phi$ channels. We found that the mean $\sqrt{\text{CRLB}}\ z_\varphi$ obtained by partially linking the photons in the 0 and π channels was the same as that obtained by linking the photons in all channels for all $\Delta\phi$ (red line and squares in Fig. 4). When $\Delta\phi = 0$, the mean $\sqrt{\text{CRLB}}\ z_\varphi$ reached its minimal value. This indicates that the localization precision achieves its optimal value when the phase shift between the p and s channels is $\pi/2$.

Since the salvaged fluorescence method with the 4Pi-SMLM system has been successfully applied to the imaging of two and three fluorophores simultaneously, we compared it to our proposed ratiometric 4Pi-SMLM method. Instead of using the salvaged fluorescence reflected by the main dichroic (ZT405/488/561/647rpcv2, Chroma) to distinguish the color, we chose a dichroic to maximize the detected photons, as shown by the dashed line in Supplement 1, Fig. 5 (ZT405/488/561/640rpcv2, Chroma). A transmittance

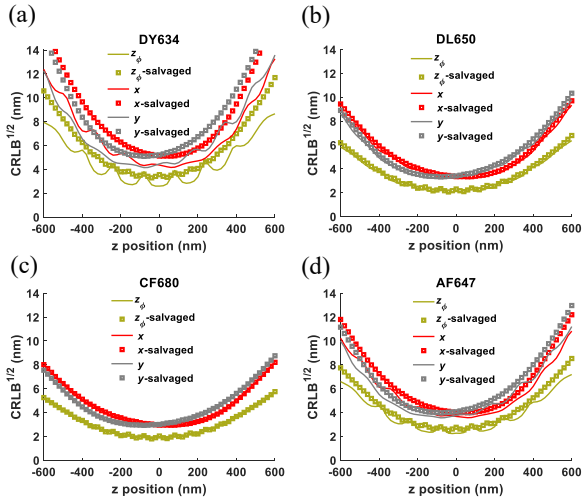

Fig. 5. Comparison of the $\sqrt{\text{CRLB}}$ values obtained using partially linked ratiometric and salvaged fluorescence multi-color imaging for different dyes: (a) DY634; (b) DL650; (c) CF680; (d) AF647. For each phase channel, 1,000 photons/localization and 20 background photons/pixel were used. Top curve (top squares), y (y-salvaged); middle curve (middle squares), x (x-salvaged); bottom curve (bottom squares), z (z-salvaged).

comparison of the new dichroic with the original dichroic can be found in Supplement 1, Table 1. The transmission fluorescence for the new dichroic was much higher than that for the original dichroic for DY634, AF647, and DL650 separately.

In order to create an intensity difference between the f^1 and f^2 channels, we additionally inserted a bandpass filter (ET710/75x, Chroma) into the f^2 channels. After inserting the filters, the photon ratio between the f^2 and f^1 channels ($\theta_{NP2}/\theta_{NP1}$) for CF680, DL650, and DY634 was 0.94, 0.75, and 0.45 respectively. For the salvaged fluorescence method, we linked all the parameters in all four channels to get optimal localization precision. For our new ratiometric 4Pi-SMLM method, we partially linked the photons in channels with a phase shift of π. As shown in Fig. 5, due to the higher photon collection efficiency and optimized parameter sharing scheme, our ratiometric 4Pi-SMLM method showed a CRLB that was better than or equivalent to that of the salvaged fluorescence method without increasing the complexity of the system.

In conclusion, we found that the photon numbers of different interference channels are highly correlated in 4Pi-SMLM and strongly affect the localization precision. Our new ratiometric multi-color 4Pi-SMLM method achieved good color assignment efficiency with minimal loss of information content within the multi-channel 4Pi-PSF, and therefore achieved optimal multi-color localization precision for 4Pi-SMLM. Especially for four-channel 4Pi-SMLM imaging, we found that the optimal resolution is obtained when the phase shift between p- and s-polarization channels is $\pi/2$. By partially linking the photons in the channels with a phase shift of π, almost no information content was lost (as indicated by the 3D CRLB) compared to the fitting scheme that links all parameters across all channels. Compared to the multi-color 4Pi-SMLM using salvaged fluorescence, our proposed method achieved higher photon collection efficiency and thus better localization precision without adding hardware complexity. Moreover, the partially linking global fitting algorithm used in this work was implemented in GPU, which is more than 38 times faster than the CPU code (Ref. [19]). We believe that this work will make multi-color 4Pi-SMLM much easier to implement in existing 4Pi microscopy, thus making better use of its ultrahigh 3D resolution imaging to investigate the spatial relationships between different biomolecules.

Funding. Natural Science Foundation of Guangdong Province (2020A1515110380); Shenzhen Municipal Science and Technology Innovation Council (KQTD20200820113012029, KQTD20170810110913065, 20200925174735005); Key Technology Research and Development Program of Shandong (2021CXGC010212); Southern University of Science and Technology.

Disclosures. The authors declare no conflicts of interest.

Data availability. The code used in this work is open source and available in Ref. [19] .

Supplemental document. See Supplement 1 for supporting content.

REFERENCES

1. E. Betzig, G. H. Patterson, R. Sougrat, O. Wolf Lindwasser, S. Olenych, J. S. Bonifacino, M. W. Davidson, J. Lippincott-Schwartz, and H. F. Hess, Science **313**, 1642 (2006).
2. M. J. Rust, M. Bates, and X. Zhuang, Nat. Methods **3**, 793 (2006).
3. X. Hao, Y. Li, S. Fu, Y. Li, Y. Xu, C. Kuang, and X. Liu, Engineering (2020).
4. G. Shtengel, J. A. Galbraith, C. G. Galbraith, J. Lippincott-Schwartz, J. M. Gillette, S. Manley, R. Sougrat, C. M. Waterman, P. Kanchanawong, M. W. Davidson, R. D. Fetter, and H. F. Hess, Proc. Natl. Acad. Sci. **106**, 3125 (2009).
5. D. Aquino, A. Schönle, C. Geisler, C. v Middendorff, C. A. Wurm, Y. Okamura, T. Lang, S. W. Hell, and A. Egner, Nat. Methods **8**, 353 (2011).
6. F. Huang, G. Sirinakis, E. S. Allgeyer, L. K. Schroeder, W. C. Duim, E. B. Kromann, T. Phan, F. E. Rivera-Molina, J. R. Myers, I. Irnov, M. Lessard, Y. Zhang, M. A. Handel, C. Jacobs-Wagner, C. Patrick Lusk, J. E. Rothman, D. Toomre, M. J. Booth, and J. Bewersdorf, Cell **166**, 1028 (2016).
7. J. Wang, E. S. Allgeyer, G. Sirinakis, Y. Zhang, K. Hu, M. D. Lessard, Y. Li, R. Diekmann, M. A. Phillips, I. M. Dobbie, J. Ries, M. J. Booth, and J. Bewersdorf, Nat. Protoc. **16**, 677 (2021).
8. C. V. Middendorff, A. Egner, C. Geisler, S. W. Hell, and A. Schönle, Opt. Express **16**, 20774 (2008).
9. M. Bates, B. Huang, G. T. Dempsey, and X. Zhuang, Science **317**, 1749 (2007).
10. R. Jungmann, M. S. Avendaño, J. B. Woehrstein, M. Dai, W. M. Shih, and P. Yin, Nat. Methods **11**, 313 (2014).
11. M. Bossi, J. Fölling, V. N. Belov, V. P. Boyarskiy, R. Medda, A. Egner, C. Eggeling, A. Schönle, and S. W. Hell, Nano Lett. **8**, 2463 (2008).
12. M. Bates, J. Keller, A. Przybylski, A. Hüper, T. Stephan, P. Ilgen, A. R. C. Delgado, E. D'Este, S. Jakobs, S. J. Sahl, and S. W. Hell, "Optimal Precision and Accuracy in 4Pi-STORM using Dynamic Spline PSF Models," bioRxiv (2021).
13. Y. Zhang, L. K. Schroeder, M. D. Lessard, P. Kidd, J. Chung, Y. Song, L. Benedetti, Y. Li, J. Ries, J. B. Grimm, L. D. Lavis, P. De Camilli, J. E. Rothman, D. Baddeley, and J. Bewersdorf, Nat. Methods **17**, 225 (2020).
14. D. Bzdok, M. Krzywinski, and N. Altman, Nat. Methods **15**, 5 (2018).
15. A. Butkute, L. Cekanavicius, G. Rimšelis, D. Gailevicius, V. Mizeikis, A. Melninkaitis, T. Baldacchini, L. Jonušauskas, and M. Malinauskas, Opt. Lett. **45**, 13 (2020).
16. S. Liu and F. Huang, Commun. Biol. **3**, 1 (2020).
17. S. Stallinga and B. Rieger, Opt. Express **18**, 24461 (2010).
18. Y. Li, W. Shi, S. Liu, U. Matti, D. Wu, and J. Ries, "Global fitting for high-accuracy multi-channel single-molecule localization," bioRxiv (2021).
19. GitHub, https://github.com/Li-Lab-SUSTech/Ratiometric-4Pi.